Biophysical Chemistry 145 (2009) 29–36

Contents lists available at ScienceDirect

Biophysical Chemistry

journal homepage: http://www.elsevier.com/locate/biophyschem

How does each substituent functional group of oseltamivir lose its activity against virulent H5N1 influenza mutants?

Thanyada Rungrotmongkol [a,b], Thanyarat Udommaneethanakit [c], Maturos Malaisree [a], Nadtanet Nunthaboot [d], Pathumwadee Intharathep [a], Pornthep Sompornpisut [a], Supot Hannongbua [a,e,*]

[a] Computational Chemistry Unit Cell, Department of Chemistry, Faculty of Science, Chulalongkorn University, Bangkok 10330, Thailand
[b] Center of Innovative Nanotechnology, Chulalongkorn University, Bangkok 10330, Thailand
[c] Nanoscience and Technology Program, Graduate School, Chulalongkorn University, Bangkok 10330, Thailand
[d] Department of Chemistry, Faculty of Science, Mahasarakham University, Mahasarakham 44150, Thailand
[e] Center of Excellence for Petroleum, Petrochemicals, and Advanced Materials, Chulalongkorn University, Bangkok 10330, Thailand

ARTICLE INFO

Article history:
Received 15 June 2009
Received in revised form 13 August 2009
Accepted 16 August 2009
Available online 22 August 2009

Keywords:
Oseltamivir resistance
H274Y
N294S
H5N1
Molecular dynamics simulations

ABSTRACT

To reveal the source of oseltamivir-resistance in influenza (A/H5N1) mutants, the drug-target interactions at each functional group were investigated using MD/LIE simulations. Oseltamivir in the H274Y mutation primarily loses the electrostatic and the vdW interaction energies at the $-NH_3^+$ and $-OCHEt_2$ moieties corresponding to the weakened hydrogen-bonds and changed distances to N1 residues. Differentially, the N294S mutation showed small changes of binding energies and intermolecular interactions. Interestingly, the presence of different conformations of E276 positioned between the $-OCHEt_2$ group and the mutated residue is likely to play an important role in oseltamivir-resistant identification. In the H274Y mutant, it moves towards the $-OCHEt_2$ group leading to a reduction in hydrophobicity and pocket size, whilst in the N294S mutant it acts as the hydrogen network center bridging with R224 and the mutated residue S294. The molecular details have answered a question of how the H274Y and N294S mutations confer the high- and medium-level of oseltamivir-resistance to H5N1.

1. Introduction

Resistance to the current influenza virus neuraminidase (NA) inhibitors is the major concern in the current treatment of patients infected with H5N1 viruses [1,2]. To date, several studies have been reported on the emergence of oseltamivir resistance, as reduced drug sensitivity, that have been associated with either the H274Y or the N294S mutations in NA subtype N1 [3–9]. Here, this study aims to understand how such mutations confer resistance to oseltamivir and is focused upon the binding affinity changes of its substituent functional groups relative to those of the wild-type strain.

Oseltamivir is the first orally active NA drug and was designed upon the transition state analog of the natural sialic acid substrate so as to inhibit the function of NA [10]. The hydroxyl and polar glycerol substitutions on the 6-membered ring of sialic acid (Fig. 1A) are replaced by amino and 3-pentyl ether groups, respectively, where the cyclohexene ring serves as oseltamivir's scaffold (Fig. 1B) [1,11]. Currently, oseltamivir is widely stockpiled in many countries for a future treatment of any influenza pandemic [2,12]. The crystal structure of oseltamivir bound to the active site residues of the native N1 is shown in Fig. 1C (cyan) [13]. Its binding residues are composed of four zones: *(i)* the arginine triad (R118, R292 and R371) and Y347, *(ii)* R152, *(iii)* E119 and D151, and *(iv)* R224 and E276 interacting with the $-COO^-$, –NHAc, $-NH_3^+$, and $-OCHEt_2$ groups of oseltamivir, respectively. The hydrophobic pocket around the bulky $-OCHEt_2$ moiety of oseltamivir is formed by the rotation of the E276's carboxylate group to bind with the guanidinium group of R224.

Oseltamivir resistances of the H274Y and N294S mutations in H5N1 were experimentally reported as a 300–1700 [3–9] and 20–80-fold [2,9] reduction in the sensitivity, respectively, compared to the wild-type. Locations of these two mutated framework residues are adjacent to E276, a residue interacting with the most hydrophobic part ($-OCHEt_2$) of the inhibitor (Fig. 1C). On the basis of the crystallographic structure data, the H274Y and N294S mutations were proposed to prevent the movement of the side chain of E276 towards the guanidinium group of R224 [2,9] and so preventing the formation of the hydrophobic pocket for accommodating oseltamivir's bulky moiety. In contrast, our results obtained from molecular dynamics (MD) simulations of oseltamivir-resistant H274Y in H5N1 [14]

* Corresponding author. Computational Chemistry Unit Cell, Department of Chemistry, Faculty of Science, Chulalongkorn University, Bangkok 10330, Thailand. Tel.: +66 22 187602; fax: +66 22 187603.
E-mail address: supot.h@chula.ac.th (S. Hannongbua).

0301-4622/$ – see front matter © 2009 Elsevier B.V. All rights reserved.
doi:10.1016/j.bpc.2009.08.006

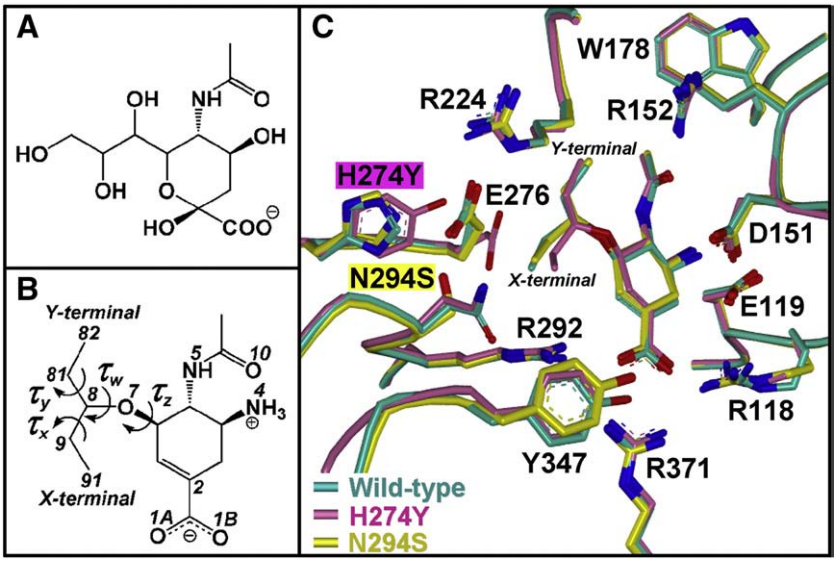

Fig. 1. Chemical structures of (A) sialic acid, and (B) oseltamivir's substituent functional groups: $-COO^-$, $-NH_3^+$, –NHAc and $-OCHEt_2$, showing the atomic numbering referred in the text. (C) The crystal structures of oseltamivir bound to the active site of native N1 (cyan), H274Y (pink) and N294S (yellow) mutants [2,13]. (For interpretation of the references to colour in this figure legend, the reader is referred to the web version of this article.)

suggest this mutation does not prevent the rotation of the E276 side chain. Instead, the source of the reduction of the hydrophobicity is due to the displacement of the E276's side chain towards the binding pocket, a notion which is well supported by the recent crystal structure of oseltamivir complexed with the H274Y mutant of H5N1 (pink in Fig. 1C) [2].

The present study has focused upon trying to understand the binding affinities of the four substituent functional groups ($-COO^-$, $-NH_3^+$, –NHAc and $-OCHEt_2$) of oseltamivir in the H274Y and N294S mutants relative to those in the wild-type. The crystallographic structures of oseltamivir complexed with the two mutants and the wild-type were examined using MD simulations in conjunction with the linear interaction energy method (LIE). Drug–target interactions were also extensively analyzed in terms of intermolecular hydrogen bonds and other specific protein-ligand distances.

2. Methods

2.1. Initial structure and system preparation

The X-ray structures of the wild-type, and the two mutant strains (H274Y and N294S), complexed with oseltamivir (OTV-N1) were obtained from the Protein Data Bank (PDB), entry codes: 2HU4 [13], 3CL0 and 3CL2 [2], respectively, and served as the starting coordinates for the three bound OTV-N1 systems: (1) OTV-WT, (2) OTV-H274Y and (3) OTV-N294S, respectively. Since crystal water molecules and Ca^{2+} ion are not present in the OTV-WT and OTV-N294S structures, they are, then, embedded into the simulated systems by superimposition with the apo-enzyme (2HTY) [13] where all water molecules which have their oxygen atoms lying within a 2.4–3.0 Å distance from the OTV-N1 heavy atoms were taken into account. Note, that the Ca^{2+} ion situated ~10 Å from the binding site is needed for the activity and stability of NA.

All calculations were performed using the Q-program package [15], version 5. The AMBER force field [16] was applied for proteins whilst the partial atomic charges and force field parameters of oseltamivir were taken from our previous calculations [17]. Each system of the OTV-N1 bound state was capped by a 25 Å sphere of TIP3P [18] water molecules centered on the C2 atom of oseltamivir (see Fig. 1B for atomic labels), and only water molecules where the oxygen was not within a 2.4 Å distance of any heavy atoms of the inhibitor and enzyme were retained. Within a 22 Å sphere of the centered C2 atom, the ionization state of each amino acid with an electrically charged side chain was assigned using the PROPKA program [19]. The ionizable residues lying at 22–25 Å distances were neutralized, except for the pairs of charged residues which probably interact via hydrogen bonds. All ionizable residues positioned further than a 25 Å sphere from the center were treated as a neutral charge. After solvation, the net charge of the final system of the OTV-N1 bound state was +2 which was then neutralized by two Cl^- ions. For the system with oseltamivir in the free state (OTV-SOL), the ligand was solvated by a 25 Å sphere of TIP3P water molecules centered on its C2 atom and counterions were added.

2.2. Molecular dynamics simulations

Spherical boundary molecular dynamics simulations of the four systems (OTV-WT, OTV-N274Y, OTV-N294S and OTV-SOL) were carried out under the surface constrained all atom solvent (SCAAS) model [20]. Harmonic constraints were treated to restrain all atoms further than 25 Å from the C2 center. Long-range electrostatic interactions were performed by the local reaction field (LRF) approximation, with a cut-off radius of 10 Å for the non-bonded interactions. To prevent the diffusion of ligand and counterions toward the edge of the simulation sphere, the position of the C2 atom of oseltamivir in the OTV-SOL system was restrained with a 100 kcal mol^{-1} $Å^{-2}$ harmonic potential, whilst a 75 kcal mol^{-1} $Å^{-2}$ flat-bottom harmonic potential, scaled from a maximum at 20.5 Å to zero at 21.5 Å from the center, was used to treat the counterions.

MD simulations of each system were set up as follows. Firstly, the positions of the water molecules were simulated, keeping all other atoms fixed to their initial positions, with the two periods of MD simulations at 5 K. Then, the whole structure was relaxed by four periods of MD simulations at 5 K and the system was heated from 5 K to 298 K in six 50 ps intervals with an increasing temperature of 50 K, and followed by equilibration phase at 298 K. Finally, four different starting structures obtained from the equilibration period were separately performed by 5-ns simulations at 298 K. The NVT ensemble was employed and the SHAKE algorithm [21] was used to constrain all bonds involving hydrogen with a simulation time step of 2 fs. Only the snapshots and energies taken from the production phase were used for the analysis.

2.3. Linear interaction energy (LIE) method

The linear interaction energy (LIE) method developed by Åqvist and co-workers [22,23] was used to calculate the binding free energies (ΔG_{bind}) of the oseltamivir bound to the NA wild-type and to the two mutant strains. This method is a linear response semi-empirical technique used to evaluate the free energy changes from the simulations of two states: *(i)* the solvated ligand (free state), and *(ii)* the ligand bound to the solvated protein (bound state). Based on the LIE method, the total binding free energy was contributed from van der Waals (U^{vdW}) and electrostatic interaction energies (U^{elec}) using the equation given below:

$$\Delta G_{bind} = \alpha\left(< U^{vdW} >_{bound} - < U^{vdW} >_{free}\right) + \beta\left(< U^{elec} >_{bound} - < U^{elec} >_{free}\right) + \gamma \quad (1)$$

where α and β are empirical scaling coefficients for van der Waals and electrostatic interaction energies, respectively, and γ is a constant. LIE is critically susceptible to α and β coefficients not being transferrable between different systems and therefore the optimized values of these coefficients derived over the series of inhibitors targeting to the NA enzyme [24] were used to fit the LIE equation in the present study. This set of coefficients has previously been found to be the most predictive model for the NA system amongst the many developed models, with or without the addition of the hydration term.

3. Results and discussion

3.1. Predicted free energy of oseltamivir binding

The predicted energies of the oseltamivir bound to the H5N1 wild-type and two mutants, H274Y and N294S, evaluated from the LIE Eq. (1) with Essex' coefficients [24] are summarized in Table 1. The experimental determined energies for the N1 inhibitory potencies by oseltamivir converted from the most recently observed K_I and IC_{50} values [2,25], are also given for comparison. In Table 1, the H274Y and N294S mutants were found to reduce the sensitivity to oseltamivir by 1.9 kcal mol^{-1} (from −11.4 to −9.5 kcal mol^{-1}) and 0.5 kcal mol^{-1} (from −11.4 to −10.9 kcal mol^{-1}), respectively. This is in good agreement with the ordering of the experimental binding energies of oseltamivir: wild-type (−13.1 or −12.1 kcal mol^{-1}) > N294S (−10.5 or −9.3 kcal mol^{-1}) > H274Y (−9.8 or −8.5 kcal mol^{-1}).

3.2. Binding free energy of each moiety of oseltamivir

To clarify how oseltamivir loses its binding affinity to the two virulent mutants relative to that of the wild-type H5N1 influenza, the binding free energies (ΔG_{bind}) contributed from the substituent functional groups (–COO$^-$, –NH$_3^+$, –NHAc and –OCHEt$_2$) were computed using the LIE equation (Eq. (1)) with the two coefficients (α = 0.472 and β = 0.122) taken from Essex's model [24]. The free energy differences ($\Delta\Delta G_{bind}$) between the mutant and wild-type strains are simply defined by:

$$\Delta\Delta G_{bind} = \Delta G_{bind}[\text{mutant}] - \Delta G_{bind}[\text{wild-type}] \quad (2)$$

where ΔG_{bind}[mutant] and ΔG_{bind}[wild-type] denote the binding free energies of each moiety against the mutant and the wild-type, respectively. Therefore, positive and negative values of $\Delta\Delta G_{bind}$ indicate that the selected moiety decreases and increases its binding affinity, respectively, to the mutation, relative to that of the wild-type. In addition, the changes of the average energy components, electrostatic and van der Waals interactions, in the bound states according to Eqs. (3a) and (3b) were evaluated, and are summarized in Table 3.

$$< \Delta\Delta U^{elec} >_{bound} = < U^{elec} >_{bound}[\text{mutant}] - < U^{elec} >_{bound}[\text{wild} - \text{type}] \quad (3a)$$

$$< \Delta\Delta U^{vdW} >_{bound} = < U^{vdW} >_{bound}[\text{mutant}] - < U^{vdW} >_{bound}[\text{wild} - \text{type}]. \quad (3b)$$

In Table 2, the contributions of individual functional group of oseltamivir to the absolute binding free energy of the wild-type complex are in the following order: –OCHEt$_2$ ~ –COO$^-$ > –NH$_3^+$ ~ –NHAc with corresponding values of −4.5, −4.1, −2.8 and −2.6 kcal mol^{-1}, respectively. The high-level resistance to oseltamivir seen in the H274Y mutant (OTV-H274Y), is correlated with the decreases in the electrostatic (9.1 kcal mol^{-1} in Table 3A) and van der Waals (1.6 kcal mol^{-1} in Table 3B) interactions. It is particularly noticeable that the –NH$_3^+$ and –OCHEt$_2$ moieties provided a much lower contribution to the intermolecular interactions between oseltamivir and the N1 enzyme, with a reduction of the binding free energies ($\Delta\Delta G_{bind}$ in Table 2) of 1.1 and 0.8 kcal mol^{-1} towards the H274Y mutant. As expected, the main contribution to the loss of the –NH$_3^+$ binding is due to the 5.5 kcal mol^{-1} reduced electrostatic interaction energy (Table 3A), whilst the loss of binding for the –OCHEt$_2$ moiety is due to the 1.6 kcal mol^{-1} lowered van der Waals interaction energy (Table 3B). By contrast, the –COO$^-$ and –NHAc groups of oseltamivir were shown to have only a small effect on the H274Y mutation, with slightly changed binding affinities to this strain ($\Delta\Delta G_{bind}$ in Table 2).

The oseltamivir-resistant N294S mutation shows a small change in the binding affinities of all four assayed functional groups of oseltamivir, 0.1–0.3 kcal mol^{-1} ($\Delta\Delta G_{bind}$ in Table 2), relative to those of wild-type. This is different from what was observed in the H274Y mutation, where a decrease in the electrostatic contribution of

Table 1
The experimental and predicted binding free energies (ΔG_{bind}) of oseltamivir to the wild-type (OTV-WT) and to the two mutants, OTV-H274Y and OTV-N294S, calculated using a MD/LIE approach with the coefficients proposed by Essex et al. [24].

System	Resistance fold[a]	ΔG_{bind} [kcal mol^{-1}]	
		Experiments[b]	Essex α = 0.472, β = 0.122, γ = 2.603 [24]
OTV-WT	–	−13.1 (−12.1)	−11.4 ± 0.4
OTV-H274Y	300–1700	−9.8 (−8.5)	−9.5 ± 0.6
OTV-N294S	20–100	−10.5 (−9.3)	−10.9 ± 0.7
rms[c]	–	–	0.8 (1.1)

The means and standard derivations are derived from four separated 5 ns simulations.
[a] Values taken from references [2–9,25].
[b] Experimental binding energies were calculated from the K_I inhibitory constants [2] and IC_{50} values [25] (the latter shown in parenthesis).
[c] The *rms* derivations were evaluated from the calculated ΔG_{bind} energies with respect to the experimental ΔG_{bind} energies derived from the K_I and IC_{50} values (the latter shown in parenthesis).

Table 2
Binding free energies (ΔG_{bind}) of the four substituent functional groups of oseltamivir (see Fig. 1B for defined partition) based on the LIE equation with Essex' coefficients (α = 0.472 and β = 0.122) [24], where $\Delta\Delta G_{bind}$ was defined in Eq. (2).

System	ΔG_{bind} [kcal mol^{-1}]			
	–COO$^-$	–NH$_3^+$	–NHAc	–OCHEt$_2$
OTV-WT	−4.1 ± 0.3	−2.8 ± 0.1	−2.6 ± 0.1	−4.5 ± 0.4
OTV-H274Y	−4.0 ± 0.5	−1.7 ± 0.2	−2.8 ± 0.3	−3.7 ± 0.7
OTV-N294S	−4.0 ± 0.4	−2.6 ± 0.3	−2.7 ± 0.3	−4.2 ± 0.7
	$\Delta\Delta G_{bind}$ [kcal mol^{-1}]			
OTV-H274Y	0.1 ± 0.8	1.1 ± 0.3	−0.2 ± 0.4	0.8 ± 1.1
OTV-N294S	0.1 ± 0.7	0.2 ± 0.4	−0.1 ± 0.4	0.3 ± 1.1

Means and standard deviation values were derived from four separated 5 ns simulations.

Table 3
Electrostatic and van der Waals interaction energy differences for oseltamivir and its moieties in the bound states of mutant and wild-type strains, as defined in Eqs. (3a) and (3b).

System	$<\Delta\Delta U^{elec}>_{bound}$ [kcal mol^{-1}]				
	Oseltamivir	–COO$^-$	–NH$_3^+$	–NHAc	–OCHEt$_2$
(A) Electrostatic interactions					
OTV-H274Y	9.1 ± 0.3	1.9 ± 0.8	5.5 ± 0.5	1.0 ± 0.4	0.7 ± 0.8
OTV-N294S	4.6 ± 0.7	3.4 ± 0.4	0.7 ± 0.6	−0.1 ± 0.4	0.5 ± 0.7
System	$<\Delta\Delta U^{vdW}>_{bound}$ [kcal mol^{-1}]				
	Oseltamivir	–COO$^-$	–NH$_3^+$	–NHAc	–OCHEt$_2$
(B) Van der Waals interactions					
OTV-H274Y	1.6 ± 0.4	−0.3 ± 0.1	1.0 ± 0.2	−0.7 ± 0.2	1.6 ± 0.4
OTV-N294S	−0.2 ± 0.4	−0.8 ± 0.1	0.3 ± 0.2	−0.1 ± 0.2	0.4 ± 0.4

Means and standard deviation values were derived from four separated 5 ns simulations.

4.6 kcal mol^{-1} (Table 3A) was found to potentially play a role in the loss of oseltamivir binding to the N294S mutation.

3.3. Loss of ligand–protein interactions

3.3.1. Around the hydrophilic side chains of oseltamivir

To monitor electrostatic intermolecular attractions, in terms of hydrogen bonds between oseltamivir and NA residues, the following two criteria were applied: *(i)* the distance between proton donor (D) and acceptor (A) atoms was less than or equal to 3.5 Å and *(ii)* the D–H..A angle was greater than or equal to 120°. The distribution plots of the D..A distance of the three simulated systems, OTV-WT, OTV-H274Y and OTV-N294S, where hydrogen bonds lay within the above criteria, are compared and shown in Fig. 2.

The intermolecular distances between the –COO$^-$ group of oseltamivir (O1A and O1B, Fig. 1B), and the N1 binding residues, are shown in Fig. 2A–E. The strong hydrogen bonding interactions with the guanidinium group of the two conserved arginines (R292 and R371) are detected in all complexes and exhibit a sharp and narrow peak centered at ~2.8 Å (Fig. 2A–D). In addition, a moderate hydrogen bond with the –OH moiety of Y347, O1A…OH(Y347), was also shown in the three simulated systems by a lower and broader peak (Fig. 2E) compared to those in Fig. 2A–D. Interestingly, the peak position for the OTV-N294S was shifted by ~0.5 Å (dashed line in Fig. 2E), indicating a weakened interaction of O1A…OH(Y347) in the N294S mutation. These results are well supported by the 3.4 kcal mol^{-1} loss of electrostatic stabilization at the –COO$^-$ group in OTV-N294S, whilst in OTV-H274Y a reduced energy of only 1.9 kcal mol^{-1} has been reported (Table 3A). Similar to our previous studies [14,17] in all N1 strains, the –COO$^-$ group of oseltamivir totally loses its interactions with the R118 residue of the arginine triad, yet this interaction is strongly detected in neuraminidase subtypes N2 and N9 [11,26,27].

A plot of the hydrogen bond distances with N4-nitrogen on the –NH$_3^+$ group of oseltamivir (defined in Fig. 1B) is shown in Fig. 2F–I. In the OTV-WT and OTV-N294S, this positively charged group was well stabilized by the two –COO$^-$ groups of E119 and D151 via the strong (a sharp peak at ~3 Å in Fig. 2F and G) and moderate (the first peak at ~2.8 Å in Fig. 2H and I) hydrogen bonding interactions. This is different from OTV-H274Y where the N4…OE1(E119) and N4…OD2 (D151) distances (Fig. 2F and I) were significantly changed, *i.e.*, the former distance was lengthened by 0.7 Å while the latter one was split into two peaks. The weakened hydrogen bonding interactions from E119 and D151 to the –NH$_3^+$ moiety of oseltamivir in OTV-H274Y, with respect to the wild-type strain, contributed a dramatic decrease in the electrostatic interaction energy of 5.5 kcal mol^{-1} (Table 3A). The other hydrogen bond detected was between the –NHAc group of oseltamivir and the guanidinium group of R152, O10…NH2(R152), as shown in Fig. 2J. Similar to the observation on the –NH$_3^+$ group, OTV-WT and OTV-N294S exhibit a very sharp peak at 2.8 Å indicating a stable and strong hydrogen bond, whilst this bond is slightly weakened in OTV-H274Y with the presence of another preferential distance at ~4.9 Å. This possibly leads to a 1.0 kcal mol^{-1} reduction of the NHAc electrostatic interaction energy in OTV-H274Y (Table 3A). With the intermolecular distances between the N1 binding residues and these two groups of oseltamivir being maintained in the N294S system, the electrostatic interaction energies were considerably similar to those obtained from the wild-type.

3.3.2. Around the hydrophobic side chain of oseltamivir

Besides hydrogen bonds, hydrophobic interactions that are likely to be responsible for accommodating the bulky –OCHEt$_2$ moiety of oseltamivir (Fig. 1C) were also considered. To investigate how the mutations at positions 274 (H274Y) and 294 (N294S) positioned next to E276 may affect the binding of oseltamivir, the interatomic distances between the –OCHEt$_2$ group and its surrounding residues, E276 and R224, and the additional residue Y347, were measured and plotted (Fig. 3), where their structural alignment of the four last snapshots taken from the 5-ns MD simulations is shown in Fig. 4.

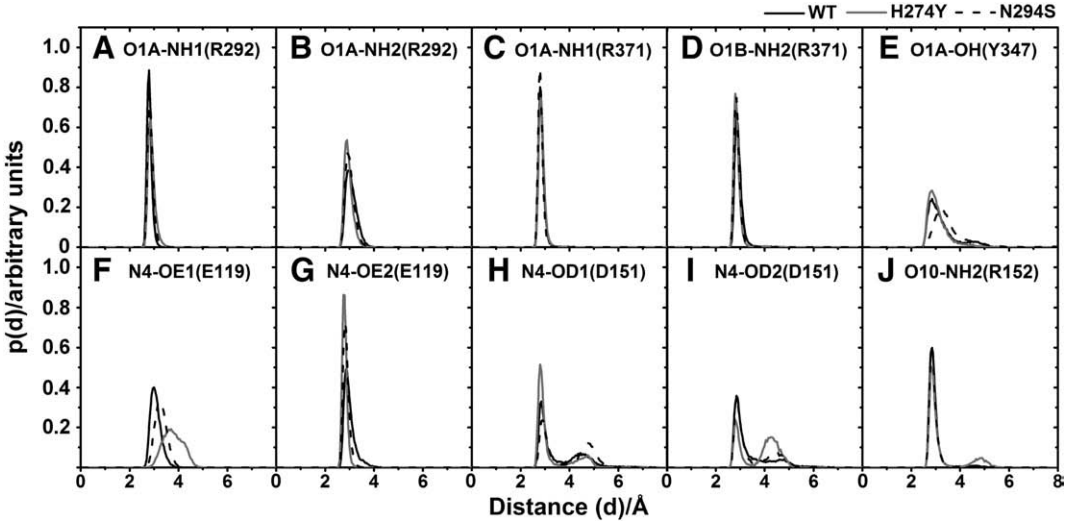

Fig. 2. The probability distributions of hydrogen bond distance between two heavy atoms of oseltamivir and its binding residues (see Fig. 1B and C for labels).

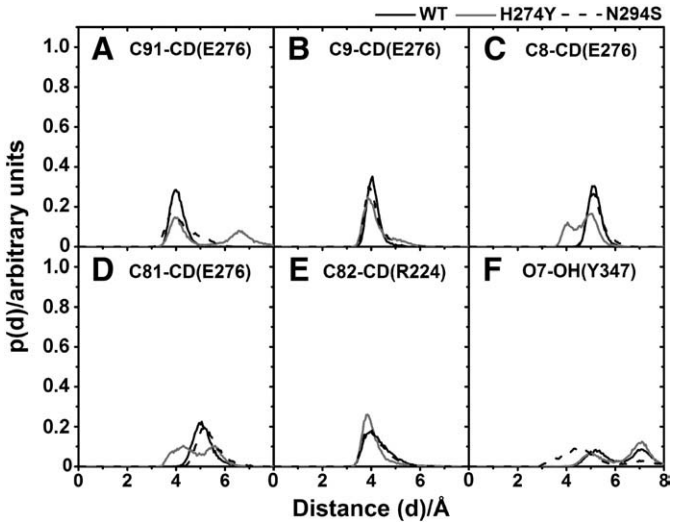

Fig. 3. The probability distributions of the distance between two specific atoms of the X- and Y-terminal of oseltamivir and the binding residues at the hydrophobic pocket (see Fig. 1B and C for labels).

The characteristics of the hydrophobic interactions between the oseltamivir's bulky group and its surrounding residues, where the peak maxima appear to be not shorter than 3 Å, were clearly displayed by the distribution plots of intermolecular distances (Fig. 3). All distance distributions involving E276 and R224 (Fig. 3A–E) in the wild-type complex show only one preferential peak. Two dramatic structural changes in the OTV-H274Y mutation complex, compared to the wild-type, were found as follows. *(i)* The phenol ring of Y274 repels the $-COO^-$ group of E276 towards one end (X-terminal) of the diethyl moiety of oseltamivir (see Figs. 1C and 4, and details in the next section), resulting in a remarkable flexibility of the $-OCHEt_2$ group which can be seen by the splitting of the C91-CD(E276) distance to form another peak at ~6.5 Å (Fig. 3A), and the broadening of the C9-CD(E276) peak to establish a long tail peak (Fig. 3B). *(ii)* A rearranged side chain of the E276 residue was observed to be more proximal to another diethyl moiety, the Y-terminal (see Figs. 1C and 4), with respect to that seen in the wild-type complex, as witnessed by the formation of the first peak of the C8-CD(E276) and C81-CD(E276) distances centered at ~4 Å (Fig. 3C and D). Consequently, such close contact possibly induces the rigidity of the probability plot of the distance between the Y-terminal and R224, leading to a sharper and narrower peak in the OTV-H274Y than in the other systems (Fig. 3F). The combined information, *(i)* and *(ii)*, implied that the size of the hydrophobic pocket for the bulky group of oseltamivir was markedly reduced in the OTV-H274Y complex, which is in good agreement with the 1.6 kcal mol^{-1} lowered van der Waal interaction energy of the $-OCHEt_2$ group (Table 3B).

For the OTV-N294S complex, the smaller residue substitution on N294 by serine directly leads to an enlargement of the hydrophobic pocket around the X-terminal (Fig. 1C), and thus allows the Y347 phenyl ring to move freely and approach closer to the bulky oseltamivir group. This can be clearly seen by the high flexibility of the Y347 phenyl ring which moves to partially occupy the enlarged hydrophobic pocket (Fig. 4B), and by the significant decrease of the distance between the O7-ester oxygen of the inhibitor and the OH-hydroxyl oxygen of the Y347 phenyl ring in the OTV-N294S complex (Fig. 3F), compared to that of wild-type. A slightly reduced hydrophobic interaction (van der Waals interaction energy) with the $-OCHEt_2$ group (0.4 kcal mol^{-1} given in Table 3B) is, therefore, a consequence of the N294S mutation.

In summary, the loss of the ligand–protein binding energies and intermolecular interactions in the NA subtype N1 H274Y and N294S mutations, is in good agreement with the observed high- and moderate-level of resistance to oseltamivir, respectively [2–9,25].

3.4. Conformational changes of the binding pocket due to mutations

To provide detailed information on the conformational changes of the binding pocket due to the mutations, the distributions of the torsional angle of the side chains of the two mutated residues (τ_{H274Y} and τ_{N294S}) and their neighborhoods (τ_{E276} and τ_{R224}), as well as the bulky $-OCHEt_2$ moiety of oseltamivir (τ_W, τ_X, τ_Y and τ_Z, see Fig. 1B for definition), were plotted (Fig. 5). The torsional angles were defined by a set of four atoms. To monitor the interaction changes between the two N1 residues, E276 and R224, as a result of the side chain rotations, hydrogen bond distances from the carboxylate group of E276 to the guanidinium group of R224 (which is known to determine the hydrophobic-pocket formation) and to the side chain of N294S were measured and the results are thus summarized and shown in Figs. 6 and 7.

In Fig. 5, the H274Y mutation cannot prevent the E276-R224 hydrogen bonding interactions or the hydrophobic-pocket formation, in contrast to the proposed mechanism of oseltamivir resistance caused by the H274Y mutation [2,9,28,29]. The primary source of resistance is more likely to be due to the reduction of the hydrophobicity and size of the hydrophobic pocket around the $-OCHEt_2$ side chain. Detailed information on the torsional angle changes (Fig. 5), is summarized as follows. The H274Y mutation confers a significant change in the side-chain torsional angle of the mutated residue 274, τ_{H274Y}, from a tilted peak dominantly found at −106° in the wild-type to a very sharp peak at −86° in the mutant (Fig. 5A). This rotation, as well as an increase in

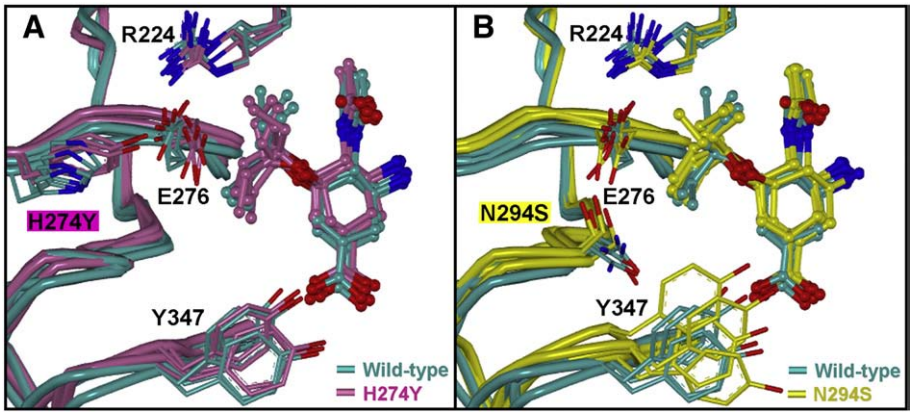

Fig. 4. Structural alignment between the four last snapshots of the 5-ns MD simulations of (A) OTV-WT and OTV-H274Y, and (B) OTV-WT and OTV-N294S. Closed view of oseltamivir, the two residues, E276 and R224, which mainly form the hydrophobic pocket around the bulky $-OCHEt_2$ group of oseltamivir, the mutated residues (H274Y and N294S) and Y347, are displayed.

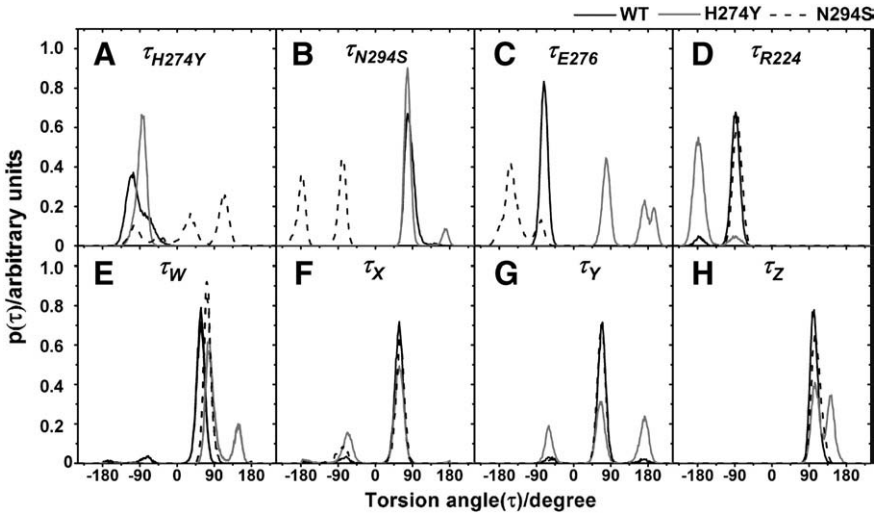

Fig. 5. Distribution plots of the torsional angle of the bulky $-OCHEt_2$ group of oseltamivir, and the side chains of two mutated residues (H274Y and N294S) and two neighboring residues (E276 and R224). See Fig. 1C for definitions.

the bulkiness of the tyrosine's phenol ring, leads to a large conformational rearrangement of the nearby residue E276 (see Fig. 1C for the initial structure and Fig. 4A for the last MD snapshots). The τ_{E276} observed in the H274Y system was noticeably split and shifted from a narrow and sharp peak at −80° for the wild-type, into two peaks at 70° and 180° (Fig. 5C). This accordingly causes the rearrangement of the R224 side-chain orientation, where τ_{R224} was found to consequently rotate by 90° (Fig. 5D) to maintain its hydrogen bonding interactions with the E276 carboxylate group, *i.e.*, the two strongly formed hydrogen bonds indicated by a sharp peak of NE(R224)-OE1(E276) and NH1(R224)-OE2(E276) at ca. 2.8 Å distance in Fig. 6A and D, respectively. These hydrogen bonds (Fig. 7B) comparable with those found in the wild-type (Fig. 7A) are in contrast to their crystal structures in which only one carboxylate oxygen (OE1) of E276 interacts with the guanidinium group of R224 (see Fig. 1C). As mentioned above, the rotations of τ_{E276} and τ_{R224} towards the inhibitor drastically reduce the hydrophobicity and size of the pocket which accommodates the bulky group of oseltamivir (see Figs. 3A–E and 4A). This is the main reason why the oseltamivir's bulky moiety cannot fit well into the hydrophobic pocket of the H274Y mutant, a notion which is also supported by the high flexibility of the four torsional angles of the particular moiety (τ_W, τ_X, τ_Y and τ_Z, Fig. 5E–H). The results are in good agreement with the previous study on the H274Y N1 mutant [30] where the Y274 phenol ring was found to push the E276 carboxylate group toward the bulky

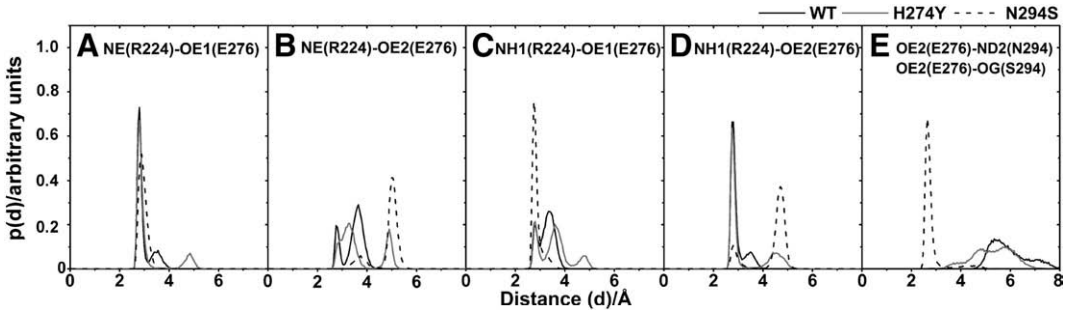

Fig. 6. Distribution plot of the hydrogen bond length of R224-E276 and E276-N294S pairs.

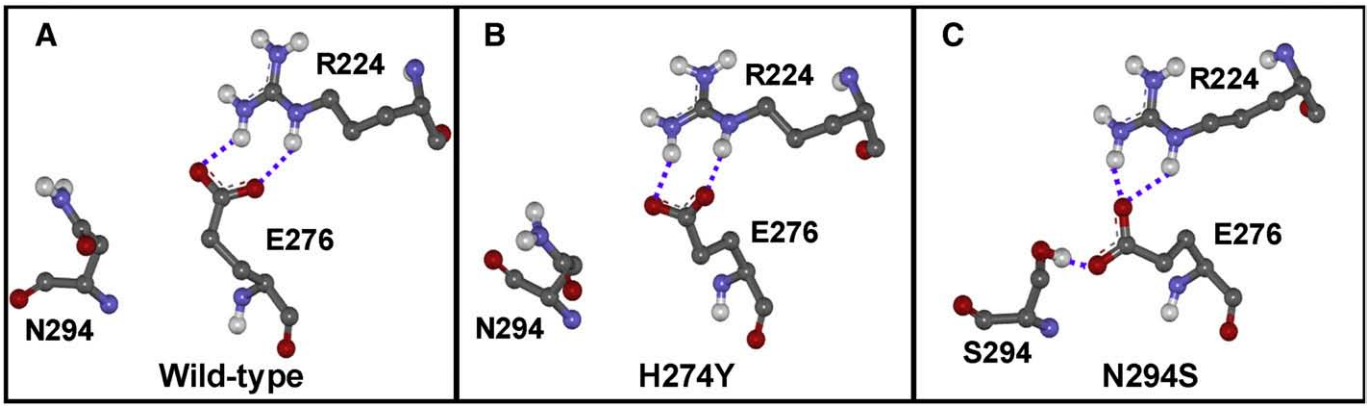

Fig. 7. Hydrogen bonds with E276 in the three simulated systems: (A) OTV-WT, (B) OTV-H274Y, and (C) OTV-N294S.

group of inhibitor; however, the hydrogen bonds between E276 and R224 were not observed.

The remarkable changes in the OTV-N294S complex were originated by the side chain rotation of the mutated residue 294 (τ_{N294S}) shifting from 78° in the wild-type to form the two preferential conformations at −80° and −180°. This leads accordingly to the primary source of oseltamivir resistance in the N294S mutated N1 strain, in contrast to that observed for the oseltamivir-resistant H274Y mutant. The N294S rotation induces the E276 side chain (τ_{E276}) to turn around in the opposite way (−78° and −152°, Fig. 5C), in comparison to that of the H274Y mutant (78° and ~180°), forming a strong hydrogen bond between the OE2-carboxylate oxygen of E276 and the OG-hydroxyl oxygen of the mutated residue S294, as indicated by the intensely sharp peak at ~3 Å in Fig. 6E, which is not detected in either the N1 wild-type or the H274Y mutant. Thus, the E276-S294 hydrogen bond formation largely prevents the side chain rotation of E276 and the strong interaction with R224 which is normally stabilized by the presence of two strong hydrogen bonds (Fig. 6A and D). In other words, only the remaining carboxylate oxygen of E276 (OE1) in the N294S system is able to form the interactions with the NE- and NH1-guanidinium nitrogens of R224 (Fig. 6A and C as well as Fig. 7C) agreeing well with the crystallographic structure (yellow in Fig. 1C). This is different from the simulations of the N294S N1 mutant [30] where the two hydrogen bonds formed between E276 and R224 were not changed (from wild-type) by the N294S mutation. Although the H274 side chain seemed to be able to rotate freely leading to the three preferential conformations at −104°, 32° and 110° (Fig. 5A), it did not interfere with the hydrophobic pocket which was constantly constructed by the hydrogen bond network around the center residue E276. Instead, the Y347 phenyl ring sometimes partially occupied the pocket (discussed above) and was also found in the crystal structure (Fig. 1C). Again, in contradiction with that observed for the high-level oseltamivir-resistant H274Y strain, the N294S mutation does not influence the conformations of the R224 side chain and –$OCHEt_2$ group. This statement was supported by the insignificant changes in their torsional angles (τ_{R224}, τ_W, τ_X, τ_Y and τ_Z in Fig. 5C and E–H), in comparison to those of wild-type. These results lead us to conclude that the hydrophobicity and size of the hydrophobic pocket were not disturbed by the N294S mutation.

4. Conclusion

In the present study, multiple MD simulations in combination with the LIE method were applied on the wild-type and the oseltamivir-resistant, H274Y and N294S, strains of avian influenza neuraminidase subtype N1. Based on the LIE model derived with Essex coefficients, the predicted inhibitory potencies of oseltamivir against all N1 strains are in good agreement with the experimental observed values. With respect to the OTV-WT complex, the $–NH_3^+$ and –$OCHEt_2$ moieties of oseltamivir dominantly lose their interactions with the H274Y mutated strain by a significantly decreased contribution of the electrostatic and the van der Waals interaction energies, respectively, attributed to the absolute binding energy of OTV-H274Y complex. Loss of interactions at these two moieties accordingly corresponded to the weakened hydrogen bond interactions and changed intermolecular distances with their neighboring residues. In contrast, the N294S mutation showed a slight change in the binding affinities of all of the functional groups of oseltamivir, and most intermolecular interactions with the N1 binding residues were likely to be maintained, except for the $–COO^-$ group with a slightly reduced hydrogen bond interaction to Y347.

The likely source of oseltamivir resistance resulting from the single mutation at the two residues positioned close to its bulky group primarily comes from different reasons. Decreases in hydrophobicity and pocket size due to the E276 rotation towards this group, where two hydrogen bonds between E276 and R224 were strongly maintained, were found in the high-level resistance to oseltamivir in the H274Y mutation. In contrast, the N294S mutation caused the E276 rotation in the opposite direction, to become the centre of the hydrogen network interacting with R224 and the mutated residue S294 which has no direct effect to the oseltamivir bulky group. The above results suggested us to propose that the potent inhibitors against the oseltamivir-resistant strains could contain the hydrophilic group, instead of the oseltamivir bulky moiety, in order to maintain the hydrogen bond interactions with the shifted E276 carboxylate sidechain in H274Y. This hydrophilic group with a longer sidechain is needed to occupy the newly formed space due to the N294S mutation.

Acknowledgements

This work was supported by The Thailand Research Fund (TRF). T.R. thanks the Post-Doctoral Program from the Commission on Higher Education and the funding for New Research (Grant No. TRG5280035) from TRF. P.S. gratefully acknowledges the support from the Emerging Diseases and Bio-Warfare project, the Center of Excellence in Clinical Virology, Chulalongkorn University. We also thank The National Center for National Nanotechnology Center for the use of the Discovery Studio.

References

[1] O. Ferraris, B. Lina, Mutations of neuraminidase implicated in neuraminidase inhibitors resistance, J. Clin. Virol. 41 (2008) 13–19.
[2] P.J. Collins, L.F. Haire, Y.P. Lin, J. Liu, R.J. Russell, P.A. Walker, J.J. Skehel, S.R. Martin, A.J. Hay, S.J. Gamblin, Crystal structures of oseltamivir-resistant influenza virus neuraminidase mutants, Nature 453 (2008) 1258–1261.
[3] J.A. Ives, J.A. Carr, D.B. Mendel, C.Y. Tai, R. Lambkin, L. Kelly, J.S. Oxford, F.G. Hayden, N.A. Roberts, The H274Y mutation in the influenza A/H1N1 neuraminidase active site following oseltamivir phosphate treatment leave virus severely compromised both in vitro and in vivo, Antivir. Res. 55 (2002) 307–317.
[4] M.Z. Wang, C.Y. Tai, D.B. Mendel, Mechanism by which mutations at His274 alter sensitivity of influenza A virus N1 neuraminidase to oseltamivir carboxylate and zanamivir, Antimicrob. Agents Chemother. 46 (2002) 3809–3816.
[5] M. Kiso, K. Mitamura, Y. Sakai-Tagawa, K. Shiraishi, C. Kawakami, K. Kimura, F.G. Hayden, N. Sugaya, Y. Kawaoka, Resistant influenza A viruses in children treated with oseltamivir: descriptive study, Lancet 364 (2004) 759–765.
[6] V.P. Mishin, F.G. Hayden, L.V. Gubareva, Susceptibilities of antiviral-resistant influenza viruses to novel neuraminidase inhibitors, Antimicrob. Agents Chemother. 49 (2005) 4515–4520.
[7] M.D. de Jong, T.T. Tran, H.K. Truong, M.H. Vo, G.J. Smith, V.C. Nguyen, V.C. Bach, T.Q. Phan, Q.H. Do, Y. Guan, J.S. Peiris, T.H. Tran, J. Farrar, Oseltamivir resistance during treatment of influenza A (H5N1) infection, N. Engl. J. Med. 353 (2005) 2667–2672.
[8] Q.M. Le, M. Kiso, K. Someya, Y.T. Sakai, T.H. Nguyen, K.H. Nguyen, N.D. Pham, H.H. Ngyen, S. Yamada, Y. Muramoto, T. Horimoto, A. Takada, H. Goto, T. Suzuki, Y. Suzuki, Y. Kawaoka, Avian flu: isolation of drug-resistant H5N1 virus, Nature 437 (2005) 1108.
[9] H.L. Yen, N.A. Ilyushina, R. Salomon, E. Hoffmann, R.G. Webster, E.A. Govorkova, Neuraminidase inhibitor-resistant recombinant A/Vietnam/1203/04 (H5N1) influenza viruses retain their replication efficiency and pathogenicity in vitro and in vivo, J. Virol. 81 (2007) 12418–12426.
[10] E. De Clercq, Antiviral agents active against influenza A virus, Nat. Rev. Drug Discov. 5 (2007) 1015–1025.
[11] M. von Itzstein, The war against influenza: discovery and development of sialidase inhibitors, Nat. Rev. Drug Discov. 6 (2007) 967–974.
[12] H.J. Schünemann, S.R. Hill, M. Kakad, R. Bellamy, T.M. Uyeki, F.G. Hayden, Y. Yazdanpanah, J. Beigel, T. Chotpitayasunondh, C. Del Mar, J. Farrar, T.T. Hien, B. Özbay, N. Sugaya, K. Fukuda, N. Shindo, L. Stockman, G.E. Vist, A. Croisier, A. Nagjdaliyev, C. Roth, G. Thomson, H. Zucker, A.D. Oxman, WHO rapid advice guidelines for pharmacological management of sporadic human infection with avian influenza A (H5N1) virus, Lancet Infect. Dis. 7 (2007) 21–31.
[13] R.J. Russell, L.F. Haire, D.J. Stevens, P.J. Collins, Y.P. Lin, G.M. Blackburn, A.J. Hay, S.J. Gamblin, J.J. Skehel, The structure of H5N1 avian influenza neuraminidase suggests new opportunities for drug design, Nature 443 (2006) 45–49.
[14] M. Malaisree, T. Rungrotmongkol, N. Nunthaboot, O. Aruksakunwong, P. Intharathep, P. Decha, P. Sompornpisut, S. Hannongbua, Source of oseltamivir resistance in avian influenza H5N1 virus with the H274Y mutation, Amino Acids (2009), doi:10.1007/s00726-008-0201-z.
[15] J. Marelius, K. Kolmodin, I. Feierberg, J. Åqvist, Q: a molecular dynamics program for free energy calculations and empirical valence bond simulations in biomolecular systems, J. Mol. Graph. Model. 16 (1998) 213–225.
[16] D.A. Case, D.A. Pearlman, J.W. Caldwell, T.E. Cheatham III, J. Wang, W.S. Ross, C.L. Simmerling, T.A. Darden, K.M. Merz, R.V. Stanton, A.L. Cheung, J.J. Vincent, M. Crowley, V. Tsui, H. Gohike, R.J. Radmer, Y. Duan, J. Pitera, I. Massova, G.L. Seibel, U.C. Singh, P.K. Weiner, P.A. Kollman, AMBER 7, University of California, San Francisco, CA, 2002.

[17] M. Malaisree, T. Rungrotmongkol, P. Decha, P. Intharathep, O. Aruksakunwong, S. Hannongbua, Understanding of known drug–target interactions in the catalytic pocket of neuraminidase subtype N1, Proteins 71 (2008) 1908–1918.
[18] W.L. Jorgensen, J. Chandrasekhar, J.D. Madura, R.W. Impey, M.L. Klein, Comparison of simple potential functions for simulating liquid water, J. Chem. Phys. 79 (1983) 926–935.
[19] H. Li, A.D. Robertson, J.H. Jensen, Very fast empirical prediction and interpretation of protein pKa values, Proteins 61 (2005) 704–721.
[20] G. King, A. Warshel, A surface constrained all-atom solvent model for effective simulations of polar solutions, J. Chem. Phys. 91 (1989) 3647–3661.
[21] J.P. Ryckaert, G. Ciccotti, H.J.C. Berendsen, Numerical integration of the Cartesian equations of motion of a system with constraints: molecular dynamics of n-alkanes, J. Chem. Phys. 23 (1997) 327–341.
[22] T. Hansson, J. Åqvist, Estimation of binding free energies for HIV proteinase inhibitors by molecular dynamics simulations, Protein Eng. 8 (1995) 1137–1144.
[23] J. Åqvist, C. Medina, J.E. Samuelsson, A new method for predicting binding-affinity in computer-aided drug design, Protein Eng. 7 (1994) 385–391.
[24] I.D. Wall, A.R. Leach, D.W. Salt, M.G. Ford, J.W. Essex, Binding constants of neuraminidase inhibitors: an investigation of the linear interaction energy method, J. Med. Chem. 42 (1999) 5142–5152.
[25] Y. Abed, B. Nehmé, M. Baz, G. Boivin, Activity of the neuraminidase inhibitor A-315675 against oseltamivir-resistant influenza neuraminidases of N1 and N2, Antivir. Res. 77 (2007) 163–166.
[26] O. Aruksakunwong, M. Malaisree, P. Decha, P. Sompornpisut, V. Parasuk, S. Pianwanit, S. Hannongbua, On the lower susceptibility of oseltamivir to influenza neuraminidase subtype N1 than those in N2 and N9, Biophys. J. 92 (2007) 798–807.
[27] P.M. Colman, J.N. Varghese, W.G. Laver, Structure of the catalytic and antigenic sites in influenza virus neuraminidase, Nature 303 (1983) 41–44.
[28] J.L. McKimm-Breschkin, A. Sahasrabudhe, T.J. Blick, M. McDonald, Mechanisms of resistance of influenza virus to neuraminidase inhibitors, Int. Congr. Ser. 1219 (2001) 855–861.
[29] A. Moscona, Oseltamivir resistance-disabling our influenza defenses, N. Engl. J. Med. 353 (2005) 2633–2636.
[30] N.X. Wang, J.J. Zheng, Computational studies of H5N1 influenza virus resistance to oseltamivir. Protein Sci. 18:707–715.